CD_3CN/CH_3CN exchange but less rapid formation of B is not obvious. However, in Rh_2^{4+} carboxylates the weakest bond is probably the M-M bond and it is not unreasonable that reaction with a chelate could lead to a change in M-M MO configuration and thereby render the metal ions substitutionally labile. For example, edge-shared bioctahedra are common for M_2L_{10} complexes and reversible formation of an activated complex of type D (Rh^{II}-Rh^{II}) or E (Rh^{III}-Rh^{I}) with a chelating ligand L-L would generate substitutional labile metal centers Rh^{II} $t_{2g}^6e_g^1$ and square-planar Rh^{I} d^8.

Detailed studies of substitution reactions at dinuclear metal centers are clearly warranted.

Acknowledgment. We thank the National Science Foundation for support and Johnson Matthey for a loan of the precious metal. R.H.C. is a National Science Foundation postdoctoral fellow, and J.M.C. is an MEC (Spain) Fulbright postdoctoral fellow.

Department of Chemistry
Indiana University
Bloomington, Indiana 47405

José M. Casas
Roger H. Cayton
Malcolm H. Chisholm*

Received August 9, 1990

Articles

Contribution from the Department of Chemistry, University of Delaware, Newark, Delaware 19716

Thermal Decomposition of Energetic Materials. 48. Structures and Decomposition Mechanisms of Copper(II) Complexes of Furazans (1,2,5-Oxadiazoles)

C. E. Stoner, Jr., A. L. Rheingold, and T. B. Brill*

Received June 8, 1990

The thermal decomposition of aminofurazan (furazan = 1,2,5-oxadiazole) complexes of Cu(II)-nitrate $[Cu(diaminofurazan)_2(H_2O)_2](NO_3)_2$ (**1**), $[Cu(furazanopiperazine)_2(CH_3CN)_2](NO_3)_2$ (**2**), and $[Cu(furazanopiperazine)_2(H_2O)_2](NO_3)_2$ (**3**) is initiated by partial displacement of H_2O or CH_3CN from the coordination sphere by NO_3^-. Proton transfer occurs forming HNO_3, some of which vaporizes. The thermal decomposition products of the complexed furazan molecule differ from the uncomplexed molecule largely because of this proton-transfer reaction. The thermal decomposition of $[Cu(furazanopiperazine)_4(H_2O)_2](ClO_4)_2 \cdot CH_3NO_2$ (**4**) is more extensive in the early stage than is the case for the analogous nitrate salts. The crystal structures of **1** and **4** show that the furazan ligand and Cu(II) bond through a ring nitrogen atom. Crystal data for **1**: monoclinic, $P2_1/c$, a = 6.382 (1) Å, b = 16.294 (4) Å, c = 7.232 (2) Å, β = 109.32 (2)°, V = 709.8 (3) Å^3, Z = 2. For **4**: orthorhombic, *Pnnm*, a = 6.596 (2) Å, b = 18.362 (8) Å, c = 14.204 (5) Å, V = 1720 (1) Å^3, Z = 2.

Introduction

The coordination chemistry of simple aminofurazans (furazan = 1,2,5-oxadiazole) is unknown. A potential ambiguity exists regarding the ligand donor site: does the amine nitrogen atom or the ring nitrogen atom or the oxygen atom serve as the Lewis base toward a transition-metal atom?

A practical aspect of aminofurazans is the fact that diaminofurazan (3,4-diamino-1,2,5-oxadiazole) suppresses the burn rate and changes the pressure dependence of combustion of rocket propellants containing NH_4ClO_4 oxidizer.[1] Several mechanisms for this effect have recently been proposed on the basis of the thermal decomposition products of diaminofurazan at high heating rates.[2] Among the products are highly thermally stable cyclic azines, such as melamine and melon. These thermally stable solids may suppress the heat and mass transfer at the burning surface.[2] The precursor compounds to the azines are NH_2CN and $[NH_4]N(CN)_2$.[2] Another mechanism is the formation of NH_3, which is known to impede the decomposition of NH_4ClO_4.[3,4]

A potential useful variation on furazan-type burn-rate modifiers might be gained by the use of metal complexes of furazans. Upon rapid decomposition of the complex, the metal center could become coordinatively unsaturated and be able to catalyze reactions in the condensed phase. At the same time the products from the furazan ligands might alter the heat and mass transfer during the surface thermolysis process. The only previously reported transition-metal complexes involving the simple furazan ligand are $ML_3(SbCl_5)_2$ salts, where L = 1,2,5-oxadiazole.[5] On the basis of electronic spectra, it was suggested that L bridges the metal atoms through its N atoms, giving octahedral coordination about M.[5] However, no crystal structures have been determined to confirm the bonding. Quadradentate chelate ligands containing diaminofurazan have recently been found to complex first-row transition-metal ions,[6-8] but these compounds are only remotely related to the ones of interest here.

Four new Cu(II) complexes of the neutral furazan ligands, diaminofurazan (DAF) and furazanopiperazine (FP), were prepared and several crystal structures were determined. DAF could

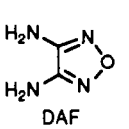

DAF

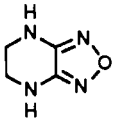

FP

bond to Cu(II) through the NH_2 groups or the ring nitrogen atom. The complexes described are $[Cu(DAF)_2(H_2O)_2](NO_3)_2$ (**1**), $[Cu(FP)_2(CH_3CN)_2](NO_3)_2$ (**2**), $[Cu(FP)_2(H_2O)_2](NO_3)_2$ (**3**), and $[Cu(FP)_4(H_2O)_2](ClO_4)_2 \cdot CH_3NO_2$ (**4**). The crystal structures of **1** and **4** and the thermal decomposition of all of the salts at slow (5 °C/min) and fast (>90 °C/s) heating rates were determined. The IR-active gas products reveal important features of the thermal decomposition mechanisms of these complexes.

(1) Chi, M.; Gleeson, B.; Hill, J.; Willer, R. L. Thiokol Corp., U.S. Patent Application 07/537658, 1990.
(2) Stoner, C. E., Jr.; Brill, T. B. *Combust. Flame*, in press.
(3) Bircumshaw, L. L.; Newman, B. H. *Proc. R. Soc. (London)* **1954**, *A227*, 155.
(4) Davies, J. V.; Jacobs, P. W. M.; Russell-Jones, A. *Trans. Faraday Soc.* **1976**, *63*, 1817.
(5) Driessen, W. L.; Everstijn, P. L. A. *Z. Naturforsch.* **1978**, *33B*, 1120.
(6) Vasil'chenko, I. S.; Kochin, S. G.; Anisomova, V. A.; Khmel'nitskii, L. I.; Garnovskii, A. D. *Khim. Geterotsikl. Soedin.* **1986**, *5*, 666.
(7) Garnovskii, A. D.; Kochin, S. G.; Minkina, L. S.; Vasil'chenko, I. S.; Konstantinovskii, L. E. *Koord. Khim.* **1989**, *15*, 258.
(8) Garnovskii, A. D.; Vasil'chenko, I. S.; Kochin, S. G.; Zeletov, V. G.; Khmel'nitskii, L. I.; Indrichan, K. M. *Koord. Khim.* **1988**, *14*, 900.

0020-1669/91/1330-0360$02.50/0

However, in no case were melamine or precursors to melamine detected, nor was NH_3 generated. Hence, any burn-rate modification of propellants by these complexes would not involve the same mechanism as the free ligands.

Experimental Section

Safety Note. Perchlorate salts of metal complexes with organic ligands are potentially explosive. Only small amounts of material should be prepared, and these should be handled with great caution.

Samples of DAF and FP were supplied by Dr. R. L. Willer (Thiokol Corp., Elkton, MD). $Cu(NO_3)\cdot 2.5H_2O$ (Fisher) and $Cu(ClO_4)_2\cdot 6H_2O$ (Aldrich) were used as received. Elemental analyses were performed by Microanalysis, Wilmington, DE.

$[Cu(DAF)_2(H_2O)_2](NO_3)_2$ (1) was prepared by adding 0.039 g (0.390 mmol) of DAF dissolved in 10 mL of warm EtOH through a frit containing excess DAF to 10 mL of a warm EtOH solution containing 0.045 g (0.195 mmol) of $Cu(NO_3)_2\cdot 2.5H_2O$. Bright green crystals of **1** formed upon evaporation. Anal. Calcd for $C_4H_{12}N_{10}O_{10}Cu$: C, 11.33; H, 2.83; N, 33.06. Found: C, 11.82; H, 2.78; N, 32.61.

$[Cu(FP)_2(CH_3CN)_2](NO_3)_2$ (2) was prepared by adding 0.23 g (1.80 mmol) of FP dissolved in 10–15 mL of warm CH_3CN dropwise with stirring to 0.21 g (0.9 mmol of $Cu(NO_3)\cdot 2.5H_2O$ dissolved in 15 mL of CH_3CN. Slow evaporation of the solution gave olive green needles, which were dried under vacuum. Anal. Calcd for $C_{12}H_{18}N_{12}O_8Cu$: C, 27.61; H, 3.45; N, 32.21. Found: C, 27.42; H, 3.53; N, 32.58.

$[Cu(FP)_2(H_2O)_2](NO_3)_2$ (3) could only be synthesized from **2**. Exposure of **2** to laboratory air gave yellow **3**. The length of time of exposure was 10–24 h for complete conversion. However, grinding **2** in air gave **3** in minutes. Anal. Calcd for $C_8H_{16}N_{10}O_{10}Cu$: C, 20.19; H, 3.36; N, 29.44. Found: C, 20.37; H, 3.44; N, 29.75.

$[Cu(FP)_4(H_2O)_2](ClO_4)_2\cdot CH_3NO_2$ (4) was prepared by dissolving 0.124 g (0.98 mmol) of FP in 10–15 mL of warm CH_3NO_2 and adding it dropwise to 0.09 g (0.25 mmol) of $Cu(ClO_4)_2\cdot 6H_2O$ dissolved in 10–15 mL of warm CH_3NO_2. The resulting brown solution yielded yellow-brown crystals upon slow evaporation. Ligand-to-metal stoichiometries of 4:1, 3:1, and 2:1 all yielded **4** as the only metal complex. The crystal structure was determined on a sample prepared with the 2:1 ligand-to-metal stoichiometry. Anal. Calcd for $C_{17}H_{31}N_{17}O_{16}Cl_2Cu$: C, 23.62; H, 3.59; N, 27.56. Found: C, 23.72; H, 3.57; N, 27.74.

$[DAFH]NO_3$ and $[FPH]NO_3$. A 0.115-g (0.91 mmol) sample of FP or 0.122 g (1.22 mmol) of DAF was dissolved in EtOH and cooled to 5 °C. A 5.7-mL aliquot of a 49:1 EtOH/concentrated HNO_3 solution was added dropwise with stirring to the FP solution. A 7.7-mL aliquot of this solution was added in the case of DAF. Crystalline salts formed upon concentration. $[FPH]NO_3$ is more stable than $[DAFH]NO_3$. The latter salt could not be dried in vacuo without loss of HNO_3, but $[FPH]NO_3$ could be dried under vacuum.

DSC and TGA Measurements. DSC and TGA studies were conducted in an Ar atmosphere on a Du Pont Instruments 2000 analyzer. The heating rate was 5 °C/min, and the sample size was about 1 mg.

IR Spectroscopy. Spectra of the solid phase were obtained on a thin film of sample prepared by burnishing or evaporating a solution on an NaCl or BaF_2 plate. If the sample was to be heated, a second plate was placed over the film and the double plate heated at 5 °C/min in a cell described before.[9] The spectra were recorded on a Nicolet 60SX FTIR at 2-cm^{-1} resolution with 36 spectra/file.

Rapid thermal decomposition studies were carried out with the rapid-scan FTIR/temperature profiling technique.[10] A 1-2-mg sample was thinly spread on the Nichrome ribbon filament. The Ar pressure in the cell was adjusted as desired between 1 and 1000 psia. The IR beam passed 3 mm above the filament. The thin film of sample was heated at a chosen rate between 90 and 200 °C/s. IR spectra of the decomposition products were recorded in real time at 10 scans/s, 2 spectra/file, and 4-cm^{-1} resolution.

X-ray Crystallography for 1 and 4. Crystals of **1** (green) and **4** (yellow-brown) were mounted on fine glass fibers. For **1**, systematic absences in the diffraction data uniquely determined the monoclinic space group $P2_1/c$. For **4**, photographic and reflection data indicated either of the orthorhombic space groups *Pnn*2 (noncentrosymmetric) or *Pnnm* (centrosymmetric). The statistical distribution for E values suggested the centrosymmetric alternative, which was supported by the chemically reasonable results of refinement. Both data sets were corrected for absorption by standard ψ-scan methods.

Both structures were solved intuitively by the placement of Cu at the origin followed by a series of difference Fourier syntheses. In **4**, a cluster of three peaks of residual electron density were located, labeled CX, CY, and CZ, which are well removed from contacts with other components of the structure and located near an inversion site, forming a six-atom group of unknown chemical identity. These atoms are not included in the calculated density. These three atoms were arbitrarily treated as half-occupancy carbon atoms and may be interpreted as disordered, substoichiometric solvent molecules. R dropped from 7.72% to the final value of 7.21% on inclusion of these peaks in the refinement model. CH_3NO_2 was proved to be present in the lattice by IR spectroscopy (vide infra).

All non-hydrogen atoms (except for CX, CY, and CZ in **4**) were anisotropically refined, and for **1**, hydrogen atoms were isotropically refined.

Atom coordinates for **1** and **4** are given in Tables II and IV, respectively. All computations used SHELXTL (5.1) software (G. Sheldrick, Nicolet XRD, Madison, WI).

(9) Karpowicz, R. J.; Brill, T. B. *Appl. Spectrosc.* **1983**, *37*, 79.
(10) Cronin, J. T.; Brill, T. B. *Appl. Spectrosc.* **1987**, *41*, 1147.

Table I. Crystallographic Data for **1** and **4**

formula	$C_4H_8CuN_8O_2\cdot 2H_2O$	$C_8H_{12}Cl_2CuN_8O_{10}\cdot 2H_2O$
fw	283.68	534.65
space group	$P2_1/c$ (No. 14)	*Pnnm* (No. 58)
a, Å	6.382 (1)	6.596 (2)
b, Å	16.294 (4)	18.362 (8)
c, Å	7.232 (2)	14.204 (5)
β, deg	109.32 (2)	
V, Å^3	709.8 (3)	1720 (1)
Z	2	2
D(calc), g/cm^3	1.327	1.032
μ(Mo, Kα), cm^{-1}	16.0	16.7
t, °C	23	23
T(max)/T(min)	1.14	1.22
λ(Mo Kα radiation), Å	0.71073	0.71073
$R(F)$, %	2.99	7.21
$R_w(F)$, %	3.38	7.91

Table II. Atomic Coordinates ($\times 10^4$) and Isotropic Thermal Parameters (Å$^2 \times 10^3$) for **1**

	x	y	z	U^a
Cu	0	0	0	20 (1)
N(1)	1552 (3)	−1045 (1)	−141 (3)	23 (1)
N(2)	4681 (3)	−1773 (1)	69 (3)	30 (1)
N(3)	−974 (4)	−2147 (1)	−674 (4)	37 (1)
N(4)	3161 (3)	−3102 (1)	−399 (4)	39 (1)
N(5)	−1933 (3)	−613 (1)	3669 (3)	23 (1)
O(1)	3842 (2)	−990 (1)	170 (3)	28 (1)
O(2)	2684 (3)	461 (1)	1919 (3)	26 (1)
O(3)	−841 (3)	−791 (1)	2590 (3)	35 (1)
O(4)	−2146 (3)	−1148 (1)	4860 (3)	37 (1)
O(5)	−2769 (3)	72 (1)	3622 (3)	41 (1)
C(1)	1034 (2)	−1825 (1)	−372 (3)	21 (1)
C(2)	3031 (3)	−2280 (1)	−255 (3)	23 (1)

[a] Equivalent isotropic U defined as one-third of the trace of the orthogonalized U_{ij} tensor.

Table III. Bond Distances and Angles for $C_4H_8CuN_8O_2\cdot 2H_2O$ (**1**)

Bond Lengths (Å)			
Cu–N(1)	1.989 (2)	N(3)–C(1)	1.334 (3)
Cu–O(2)	1.963 (2)	N(4)–C(2)	1.347 (3)
N(1)–O(1)	1.406 (2)	N(5)–O(3)	1.240 (3)
N(1)–C(1)	1.310 (3)	N(5)–O(4)	1.264 (3)
N(2)–O(1)	1.395 (2)	N(5)–O(5)	1.233 (3)
N(2)–C(2)	1.297 (3)	C(1)–C(2)	1.453 (3)
Bond Angles (deg)			
N(1)–Cu–O(2)	91.8 (1)	O(3)–N(5)–O(5)	121.5 (2)
N(1)–Cu–N(1A)	180.0 (1)	O(4)–N(5)–O(5)	120.0 (2)
O(2)–Cu–N(1A)	88.2 (1)	N(1)–O(1)–N(2)	109.2 (1)
O(2)–Cu–O(2A)	180.0 (1)	N(1)–C(1)–N(3)	126.2 (2)
Cu–N(1)–O(1)	116.5 (1)	N(1)–C(1)–C(2)	107.9 (2)
Cu–N(1)–C(1)	136.7 (2)	N(3)–C(1)–C(2)	125.8 (2)
O(1)–N(1)–C(1)	106.7 (2)	N(2)–C(2)–N(4)	125.4 (2)
O(1)–N(2)–C(2)	106.9 (2)	N(2)–C(2)–C(1)	109.2 (2)
O(3)–N(5)–O(4)	118.4 (2)	N(4)–C(2)–C(1)	125.3 (2)

Crystal Structures of 1 and 4

Figures 1 and 2 show the structure of the Cu(II) complex of **1** and **4**, respectively. Hathaway's (4 + 0 + 2*) arrangement of

Table IV. Atomic Coordinates ($\times 10^4$) and Isotropic Thermal Parameters ($Å^2 \times 10^3$) for **4**

	x	*y*	*z*	*U*[a]
Cu	5000	10000	5000	23.3 (3)*
Cl	4476 (4)	7418 (1)	5000	39.7 (7)*
N(1)	3637 (6)	9425 (2)	3971 (3)	27 (1)*
O(2)	1511 (5)	9378 (2)	3969 (3)	40 (1)*
N(3)	870 (8)	8998 (3)	3157 (4)	49 (2)*
C(4)	2522 (9)	8834 (3)	2697 (4)	38 (2)*
C(5)	4260 (8)	9101 (3)	3207 (4)	27 (1)*
N(6)	6163 (7)	9033 (3)	2860 (4)	41 (2)*
C(7)	6414 (13)	8559 (5)	2078 (7)	75 (3)*
C(8)	4632 (12)	8454 (8)	1471 (7)	109 (5)*
N(9)	2734 (9)	8458 (4)	1891 (4)	61 (2)*
Ow(1)	7635 (8)	9113 (3)	5000	39 (2)*
O(5)	4425 (17)	6658 (4)	5000	97 (4)*
O(6)	2673 (21)	7766 (7)	5000	191 (10)*
O(7)	5276 (21)	7670 (4)	5755 (9)	248 (7)*
CX	0	0	896 (22)	149 (9)
CY	1074 (47)	−19 (16)	0	176 (12)
CZ	2628 (81)	−56 (26)	0	326 (29)

[a] Asterisk denotes atoms were refined by using the equivalent isotropic *U* defined as one-third of the trace of the orthogonalized U_{ij} tensor.

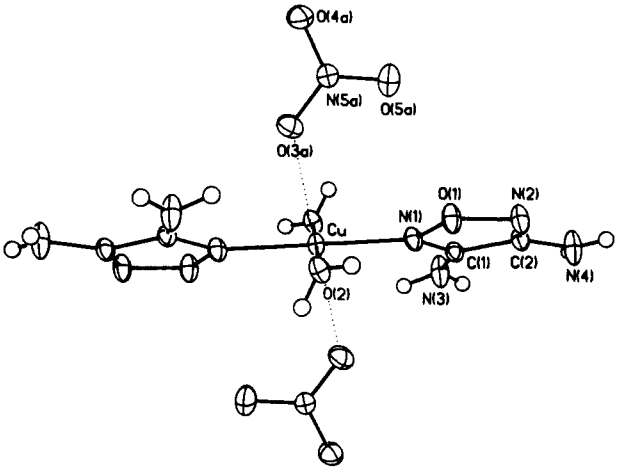

Figure 1. Structure of $[Cu(DAF)_2(H_2O)_2](NO_3)_2$ (**1**) showing 30% probability thermal ellipsoids.

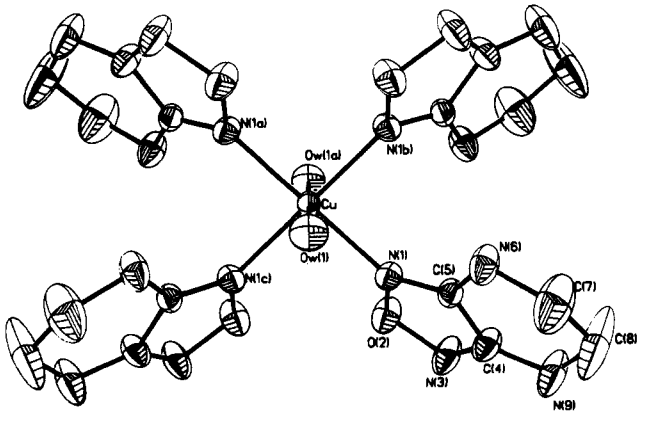

Figure 2. Structure of the complex cation of $[Cu(FP)_4(H_2O)_2](ClO_4)_2 \cdot CH_3NO_2$ (**4**) showing 30% probability thermal ellipsoids.

ligands typical of Cu(II)[11,12] forms in these compounds. Two H_2O molecules bond to the metal in both complexes, but four furazan ligands coordinate in **4** while only two coordinate in **1**. NO_3^- occupies the remaining two sites of **1**. The different number of coordinated furazan ligands is attributable to the competition

(11) Hathaway, B. J. *Struct. Bonding (Berlin)* **1973**, *14*, 49.
(12) Hathaway, B. J. *Struct. Bonding (Berlin)* **1984**, *57*, 107.

Table V. Bond Distances and Angles for $C_8H_{12}Cl_2CuN_8O_{10} \cdot 2H_2O$ (**4**)

Bond Lengths (Å)			
Cu–N(1)	2.014 (4)	Cu–Ow(1)	2.382 (6)
Cl–O(5)	1.395 (7)	Cl–O(6)	1.350 (14)
Cl–O(7)	1.282 (12)	N(1)–C(5)	1.305 (7)
N(1)–O(2)	1.405 (5)	N(3)–C(4)	1.306 (8)
O(2)–N(3)	1.412 (7)	C(4)–N(9)	1.344 (9)
O(4)–C(5)	1.442 (8)	N(6)–C(7)	1.421 (11)
C(5)–N(6)	1.354 (7)	C(8)–N(9)	1.387 (10)
C(7)–C(8)	1.470 (12)		

Bond Angles (deg)			
N(1)–Cu–Ow(1)	88.1 (1)	N(1)–Cu–N(1B)	87.0 (2)
Ow(1)–Cu–N(1A)	91.9 (1)	Ow(1)–Cu–Ow(1A)	180.0 (1)
N(1)–Cu–N(1C)	93.0 (2)	O(5)–Cl–O(6)	116.9 (8)
O(5)–Cl–O(7)	111.8 (5)	O(6)–Cl–O(7)	101.0 (6)
O(7)–Cl–O(7A)	113.6 (11)	Cu–N(1)–O(2)	118.7 (3)
Cu–N(1)–C(5)	134.6 (4)	O(2)–N(1)–C(5)	106.5 (4)
N(1)–O(2)–N(3)	109.3 (4)	O(2)–N(3)–C(4)	105.9 (5)
N(3)–C(4)–C(5)	109.5 (5)	N(3)–C(4)–N(9)	129.2 (6)
C(5)–C(4)–N(9)	121.3 (5)	N(1)–C(5)–C(4)	108.8 (5)
N(1)–C(5)–N(6)	129.5 (5)	C(4)–C(5)–N(6)	121.6 (5)
C(5)–N(6)–C(7)	116.6 (5)	N(6)–C(7)–C(8)	116.5 (8)
C(7)–C(8)–N(9)	117.9 (8)	C(4)–N(9)–C(8)	117.6 (7)
N(1)–Cu–N(1A)	180.0 (1)		

between the coordinating powers of the furazan ligand, NO_3^-, and ClO_4^-. The furazan has a relatively low donor power[5] so that two NO_3^- can compete effectively for the coordination sites on Cu(II). On the other hand, ClO_4^- has an even lower tendency to coordinate to Cu(II) and so the furazan ligand competes effectively and is able to occupy four coordination sites.

DAF tilts 32.3° out of the $CuN_2(H_2O)_2$ plane. The main reason for this tilt appears to be that the cations stack in the lattice with the DAF ligands face-to-face. The $Cu(H_2O)_2$ vector, in effect, tilts by 32.2° to allow the axial NO_3^- ions to bond to Cu(II) but to avoid one another in neighboring cations. This packing demand also affects the angles in the Cu(II) coordination sphere. While the angles about Cu(II) in the $CuN_2(H_2O)_2$ plane are 90 ± 1, the $Cu(ONO_2)_2$ vector is canted 10° from a line perpendicular to the plane. Intramolecular hydrogen bonding appears to play a minor role in the structural details. The efficiency of stacking of the cations in the crystal lattice of **4** also is the main reason the FP ligands do not alternate "up–down", as might be expected from intramolecular steric considerations, but are "up–up–down–down".

The effect of coordination to Cu(II) on the internal bond distances and angles of FP and DAF can be analyzed by comparison with the uncomplexed DAF molecule[13] and dinitrofurazano[3,4-*b*]piperazine (**5**).[14] The distances and angles in

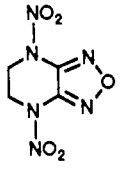

5

Tables III and V show that the structures of the furazan rings of **1** and **4** are very similar. Moreover, the bond distances and angles are the same as those in pure DAF within experimental error.[13] The average furazan C–N bond distance of **1** and **4** [1.31 (1) Å] is shorter than the partial C–N double bonds of heterocyclic rings (1.35 Å).[15] The average C–C bond [1.44 (1) Å] is intermediate between typical C–C (1.54 Å) and C=C distances (1.34 Å).[15] The average N–O bond distance [1.41 (1) Å] is typical of an N–O single bond (1.40 Å).[16] Thus, π-electron delocalization

(13) Batsanov, A. S.; Struchkov, Yu. T. *J. Struct. Chem. (Engl. Transl.)* **1988**, *26*, 52.
(14) Oyumi, Y.; Rheingold, A. L.; Brill, T. B. *J. Phys. Chem.* **1986**, *90*, 4686.
(15) *CRC Handbook of Chemistry and Physics*; Weast, R. C., Ed.; CRC Press: Boca Raton, FL, 1989; p F188.

occurs over the C_2N_2 portion of the furazan ring. The C–NH_2 groups of DAF and C–N bonds of the piperazine ring of FP that connect to the furazan ring are included in the π-electron delocalization through the lone pair on the amine nitrogen atom. This is apparent from the relatively short average C–N bond distance [1.34 (1) Å]. Thus, the π-electron system of these ligands is represented by **6**. As a result of **6**, the amine hydrogen atoms

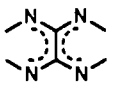

6

of **1** are located in the plane of the heavy atoms of DAF. The absence of a stereochemically active lone electron pair on the amine nitrogen atoms explains why these atoms are not the donor sites when DAF coordinates to Cu(II).

The average bond distances within the furazan ring are shorter for **5** [1.354 (3) Å] than for **4** [1.373 (4) Å], while the average C–N distance connecting the furazan ring to the amine nitrogen atoms is longer in **5** [1.390 (3) Å] than in **4** [1.347 (4) Å]. This pattern indicates that the π-electron density of the furazin ring is greater when less has to be shared with the exo C–N bonds. The lower π-electron density in the exo C–N bonds of **5** compared to the case of **4** is caused by the NO_2 groups of **5** which π-bond with the amine lone pair.

The above comparisons of the internal bond distances and angles of **1**, **4**, **5**, and free DAF indicate that coordination of the furazan ring to Cu(II) does not significantly change the structure of the ring. On the other hand, the Cu–N bond distances of **1** and **4** are typical (ca. 2.0 Å)[16] so that the Cu–N bond does not appear to be structurally weak. However, as described below, a portion of the furazan ligands volatilizes intact when **1** and **4** are rapidly heated.

Thermal Decomposition

The decomposition of these furazan–metal complexes is the main property of interest for application in burn-rate modification. Combustion conditions involve a high heating rate and superatmospheric pressure so that the most useful mechanistic information comes from studies approximating these conditions. However, slow heating rate studies can be helpful if the same processes can be shown to occur at high heating rates.

$[Cu(DAF)_2(H_2O)_2](NO_3)_2$ (1). Figure 3 shows that major changes occur in the mid-IR spectrum of **1** between 80 and 105 °C. ν_3 of the weakly coordinated NO_3^- ion at 1437 cm^{-1} diminishes, while new peaks appear at 1482 and 1292 cm^{-1}. This indicates removal of the E degeneracy of ν_3 of NO_3^- as it forms a stronger bond to the metal. The furazan modes in the 1560–1700- and 1350-cm^{-1} range broaden and become less resolved at higher temperature, indicating that the crystal lattice is strongly disrupted. Thus, the IR spectrum shows that the first step of thermal decomposition of **1** is displacement of at least one H_2O from the Cu(II) coordination sphere by at least one NO_3^- ion. This description is consistent with the TGA, which reveals the weight loss corresponding to 1 equiv of H_2O beginning at about 95 °C. Also, DSC reveals a broad endotherm beginning at about 80 °C followed by an exotherm at 104 °C (226 ± 19 J/g). Rapid decomposition of the complex occurs at about 120 °C in both the DSC and TGA measurements.

The decomposition temperature of **1** is 100 °C below that of pure DAF.[2] The gas products evolved at high heating rates (≥60 °C/s) suggest why. HNO_3, H_2O, and HNCO are the first detected products from **1** and appear simultaneously at the decomposition exotherm. The H_2O is released when it is displaced from the coordination sphere by NO_3^-. HNO_3(g) forms by proton transfer to NO_3^- in the condensed phase followed by desorption. Hence, displacement of H_2O by some of the NO_3^- ions and H^+ transfer to other NO_3^- ions to form HNO_3 are parallel steps that occur in the first phase of decomposition of **1**. Neither of these reactions is available to pure DAF. Unassisted ring opening is required in the decomposition of DAF and occurs at a higher temperature (225 °C).

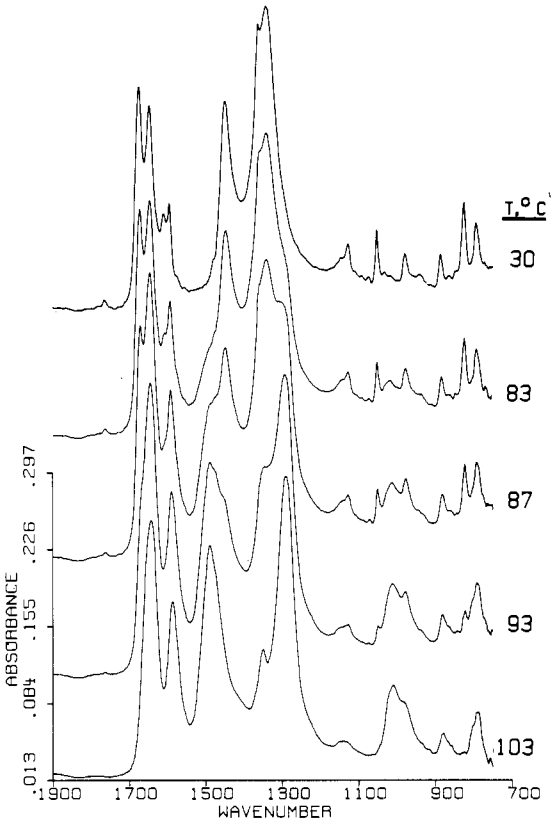

Figure 3. Selected mid-IR spectra of **1** heated at 5 °C/min showing the movement of at least one of the NO_3^- ions from a weakly coordinated state to a more strongly coordinated position.

The HNCO formed by **1** is probably a direct fragment of the furazan ring, but it is informative that HNCO is not produced by pure DAF. On the other hand, NH_3 is formed by DAF but not **1**. These differences are consistent with the NH_2 groups being the source of H^+ that releases HNO_3(g) from **1**. The >C=NH^- group that remains can be the source of HNCO after reaction with an oxygen source. The oxygen source is most likely the HNO_3 formed in the condensed phase. The liberation of N_2O and NO by **1** is consistent with oxygen-transfer reactions occurring with HNO_3. The formation of NH_3 from pure DAF and not **1** also fits this interpretation. If some of the N–H_2 bonds cleave to form HNO_3, then they are not available to form NH_3. This is compounded by the oxidizing environment caused by the presence of HNO_3 in the condensed phase that favors the formation of NO, N_2O, and HNCO rather than NH_3.

Fast thermolysis of **1** also releases some intact DAF(g). Hence, ring opening and Cu–N bond cleavage occur simultaneously. The reaction branch leading to the decomposition gas products appears to be much more important than that leading to ligand volatilization based on the absorbance intensities (Figure 4). At Ar pressures of 15 psia and higher the DAF(g) reacts with HNO_3(g) to form an aerosol of $[DAFH]NO_3$. This salt was identified by comparison with an authentic sample. Figure 4 shows the gas products from **1** at 2 and 15 psia Ar compared to the gas phase above a sample of $[DAFH]NO_3$. The formation of DAF(g) is consistent with the 1,2,5-oxadiazole ring being a relatively weak Lewis base toward transition metals.[5] Unlike pure DAF, there is no evidence that NH_2CN, $[NH_4]N(CN)_2$, or any other product that could lead to melamine forms during the thermolysis of **1**. This is consistent with the evidence described above that the NH_2 groups degrade in the proton-transfer step leading to HNO_3.

$[Cu(FP)_2(CH_3CN)_2](NO_3)_2$ (2) and $[Cu(FP)_2(H_2O)_2](NO_3)_2$ (3). H_2O spontaneously displaces CH_3CN, giving yellow **3**, when green **2** is exposed to air. The conversion time requires 10–24 h. Diffraction-quality crystals could not be grown for either complex. However, the thermal decomposition of complexes **1–3**

(16) Huheey, J. E. *Inorganic Chemistry*; Harper and Row: New York, 1983.

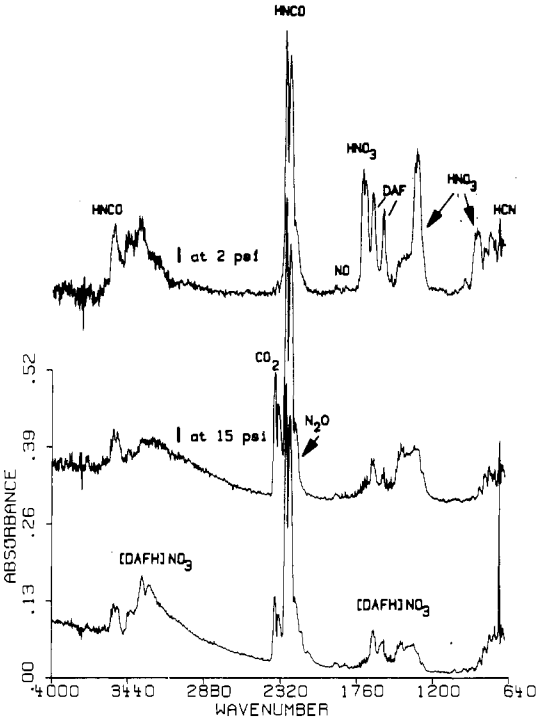

Figure 4. IR spectra of the gas phase above **1** heated at 100 °C/s under 2 and 15 psia Ar compared to the spectrum of $[DAFH]NO_3$ aerosol (bottom) which was formed by rapid heating of $[DAFH]NO_3$ at 15 psia Ar.

have much in common. Given the similar stoichiometries, it is probable that their molecular structures are similar.

2 loses weight corresponding to 1 equiv of CH_3CN beginning at about 125 °C according to TGA. Steep weight loss due to decomposition of the complex begins at about 150 °C. By DSC an endotherm begins at 125 °C followed by the decomposition exotherm at about 150 °C (340 ± 40 J/g). **3** begins to lose H_2O at about 75 °C, as indicated by both TGA and DSC. It has a decomposition exotherm at about the same temperature as **2** (160 °C, 400 ± 40 J/g), suggesting that the linkages that are key to rapid decomposition have become similar at the decomposition point. Thus, it is probable that the same early reaction sequence that occurs in **1** also occurs in **2** and **3**, i.e. that some of the NO_3^- ions displace CH_3CN and H_2O from the Cu(II) coordination sphere. The partially desolvated complex then releases decomposition product gases.

Figure 5 shows the gas products that are formed by **2** heated at 100 °C/s under 2 psi Ar along with the spectrum of solid FP. The first detected gas product is CH_3CN. $HNO_3(g)$ is the second product, indicating that proton transfer occurs. The same result is obtained with **3** except that H_2O rather than CH_3CN is the first detected gas product. HNCO, CO_2, NO, HCN, and N_2O then appear together as a result of the redox reactions between HNO_3 and the ligand in the condensed phase. However, intact FP is also evolved due to Cu–N bond heterolysis. If the Ar pressure is 15 psia or greater, then $[FPH]NO_3$ aerosol is formed by recombination in the gas phase. If the NH_2 groups of **1** play a role in the proton transfer leading to $HNO_3(g)$, as proposed above, then it is understandable why **2** and **3** are more thermally stable than **1**.

$[Cu(FP)_4(H_2O)_2](ClO_4)_2 \cdot CH_3NO_2$ (4). The decomposition process of **4** is different from the nitrate salts discussed above.

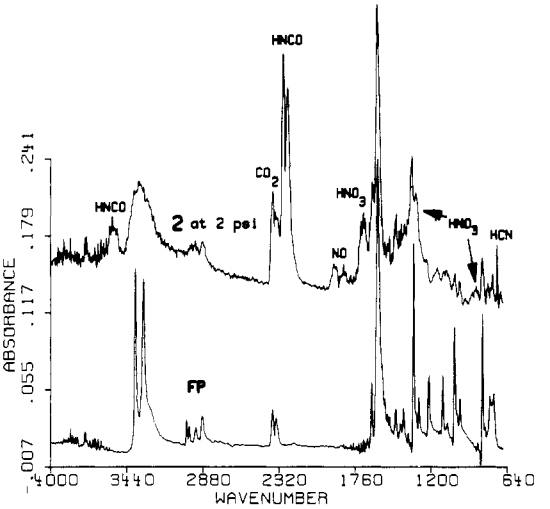

Figure 5. IR spectra of the near-surface gas products 1.76 s after the onset of heating when **2** is heated at about 100 °C/s under 2 psia Ar. The gas products are compared to the solid-phase spectrum of pure FP to show that some FP is evolved from complex **2**.

4 evolves the CH_3NO_2 of crystallization at about 120 °C, according to the TGA. This produces a broad DSC endotherm. The DSC and TGA then reveal two broad decomposition steps (135–230 °C, 1100 J/g; 240–320 °C, 1200 J/g). The weight changes in these steps do not correspond to the loss of any single entity of **4**. Consistent with this, the IR spectrum of the gases at fast heating rates shows CH_3NO_2 as the initial product, but H_2O, HNCO, N_2O, NO, CO, CO_2, HCN, CH_4, and C_2H_4 then all appear simultaneously. No $HClO_4$ or HCl is detected, suggesting that the residue contains copper chloride or that Cl_2 forms. No FP is detected in the gas phase so that the redox reactions involving ClO_4^- and the cation destroy all of the FP before any can volatilize. Both the energy and the gas products indicate that the decomposition reactions of **4** are more extensive than those of **1–3**.

Conclusions

Some of the key steps of the complicated thermal decomposition process of these complexes come to light by the combination of data from DSC, TGA, IR spectroscopy, and X-ray crystallography. The evolved gases show why melamine-like cyclic azines would not be expected to form upon rapid decomposition of **1–4**. Cyclic azines require that NH_2CN or $[NH_4]N(CN)_2$ form first and then self-react. In complexes **1–4** the amine groups of the aminofurazan ligands appear to engage in proton transfer in the induction step so that HNCO forms instead of NH_2CN. Therefore, the only source of melamine-like products is the free ligand that volatilizes from the nitrate salt complexes. The fact that NH_3 is also not detected suggests that these metal–furazan complexes would not affect the burn-rate of NH_4ClO_4-containing propellants in the same way as the furazan compounds alone.

Acknowledgment. We are grateful to Dr. R. L. Willer for supplying samples of DAF and FP for this work. We also thank the Thiokol Corp. and Dr. D. A. Flanigan for support on an independent research and development program.

Supplementary Material Available: For **1** and **4**, listings of full crystallographic data, anisotropic thermal parameters, and hydrogen atom coordinates (4 pages); structure factor tables for **1** and **4** (18 pages). Ordering information is given on any current masthead page.